

Contextual Filtering of CT Images Using Markovian Wiener Filters With a Non Local Means Approach for Statistical Estimation

Denis H. P. Salvadeo, Nelson D. A. Mascarenhas, Alexandre L. M. Levada
Computer Department
Federal University of São Carlos (UFSCar)
São Carlos, Brazil
Email: {denissalvadeo, nelson, alexandre}@dc.ufscar.br

Abstract—Recently, investigations on medical imaging have been indicating a strong correlation between cases of cancers and the increasing number of Computed Tomography (CT) exams, mainly due to high radiation doses to which patients are exposed during the data acquisition process. Thus, there is a need to reduce the radiation doses whereas still keeping satisfactory quality images for diagnosis. In this paper, we propose to filter noise in CT images using contextual versions of Wiener Filter such as Generalized Wiener Filter (GWF) and Non Local Means approach for parameter estimation. Experiments show that the proposed methods are promising, since they provide good results with no significant increase in the computational cost.

Keywords—Wiener Filter; Fisher Information; Markov Random Fields; Non Local Means Approach; Image Denoising; Computed Tomography.

I. INTRODUCTION

Computed Tomography (CT) technology has been used in several areas, especially in medical sciences for diagnosis purposes, such as the detection of some kinds of cancer (e. g., in the lungs). However, in the last years, due to the excessive use of this technology, by the emission of high doses of radiation, there has been an increase in cases of cancers related to CT [1]. Thus, a reduction on the radiation doses in CT imaging has become a fundamental concern among radiologists worldwide. But, as a side effect, lowering radiation doses causes a decrease in the signal-to-noise ratio (SNR).

On lower doses, low photon counting due to the short exposure time to the tomograph rays degrades the CT projections with Poisson noise [2], [3]. Although it is acknowledged that a general model for the noise in the reconstructed image is still lacking [4], [5], by invoking the Central Limit Theorem [3], we adopt the simplified model of a Gaussian, white, additive and signal independent noise. The good experimental results that were obtained tend to justify this simplifying assumption.

Thus, in this paper, we propose denoising in CT image domain. The images are first reconstructed from the CT projections by using the FBP (Filtered Backprojection) algorithm [2] or a POCS (Projections Onto Convex Sets) based algorithm [6], [7], [8]. In the case of POCS, it is noteworthy that a very low percentage of object pixels is subject to the nonlinear constraints of non-negativity and finite support,

considered in this algorithm. Therefore, the arguments for using the Central Limit Theorem are still valid.

Then, in the image domain, we assume an Additive White Gaussian Noise (AWGN) model, and denoising is performed by using a Wiener filter generalization that is based on Fisher Information minimization, a concept that tries to maximize the likelihood of contextual configuration patterns (patches), relating the Pointwise Wiener Filtering (WF) and Gaussian-Markov Random Fields (GMRF's). The a priori statistics for this bayesian approach is obtained by a prefiltered image through a Non Local Means filter.

The paper is organized as follows: Section 2 briefly introduces the basis of MRF theory. Section 3 presents the Wiener Filter and Wiener Filter with Separable (SWF) and Isotropic MRF's (IWF) that are used for comparisons. Sections 4 and 5 explain the GWF method and the Non Local Means method, respectively. Section 6 presents the proposed methodology. Section 7 describes the experiments and shows the results, respectively. Finally, Section 8 presents some conclusions and future works.

II. MARKOV RANDOM FIELDS (MRF)

Markov Random Fields are defined on a neighborhood system satisfying two conditions: the conditional probability of a certain random variable in the field given all the others depends exclusively of its neighbors and any realization of the field has probability higher than zero [9], [10].

In practical terms, the most important result regarding practical MRF applications is given by the Hammersley-Clifford Theorem [9]. Basically, it establishes the equivalence between MRF and Gibbs Random Fields (GRF), such that we can obtain the joint distribution of the field from the local conditional probabilities (and vice-versa). This implies that the last can be given in terms of clique potentials [9] that correspond to a function of the random variables of the field. In this work, MRF will define a smoothness constraint in the form of a priori knowledge.

III. CLASSICAL WIENER FILTERS

The Wiener filter is the optimum filter in the sense of the Linear Minimum Mean Square Error (LMMSE) estimate of

a target signal given an observed signal. There are several approaches for Wiener filter based on different image formation models. In this Section, three approaches are considered: Pointwise, Isotropic and Separable MRF Wiener filters.

The Pointwise Wiener Filter corresponds to a local LMMSE estimate. Here, we use a version proposed by Kuan et al [11] for additive, zero-mean noise that is represented by the following equation

$$\hat{f}(i, j) = \bar{f}(i, j) + \frac{\sigma_f^2(i, j)}{\sigma_f^2(i, j) + \sigma_v^2(i, j)} (g(i, j) - \bar{g}(i, j)), \quad (1)$$

where $\hat{f}(i, j)$ is the estimated noise-free pixel, $g(i, j)$ is a current observed pixel, $\bar{f}(i, j)$ and $\bar{g}(i, j)$ corresponds to the local means of original and observed (noisy) image, respectively and $\sigma_f^2(i, j)$ and $\sigma_v^2(i, j)$ are the local variances of original image and noise, respectively. Local estimates for mean and variance can be obtained in a window of $W \times W$ size. Since we are assuming zero mean additive noise, we consider that $\bar{g}(i, j) = \bar{f}(i, j)$. In addition, since only the observed image is available, to obtain an estimate of $\bar{f}(i, j)$ and $\sigma_f^2(i, j)$, a mean filter is applied on the noisy image to obtain an approximation of the original image. Also, as we consider noise-independent signal, $\sigma_v^2(i, j)$ is constant over all pixels.

The other two filters embed Markov Random Fields in the derivation of the LMMSE estimate that is based on the Orthogonality Principle (OP) [12]. Assuming that the image formation model is additive and that there is no correlation between noise and image, we obtain the input and output autocorrelations, denoted by R_{ff} and R_{gg} , respectively. To obtain the LMMSE estimate by OP, we must to solve the following equation (in a matrix form) for each pixel in the image:

$$R_{gg}\alpha = R_{fg}, \quad (2)$$

where α is an unknown vector to be calculated and R_{fg} is the cross-correlation between original and observed image, denoted by f and g , respectively.

In addition, it is worth noting that each line in R_{gg} corresponds to the autocorrelation in g between each point and all others regarding a window with size W by W pixels, thus R_{gg} is a N by N matrix, where $N = W \times W$. On the other hand, R_{fg} is a column vector with size $N \times 1$ that represents the crosscorrelation of f and g , between the central (current) pixel and the others in the window.

With the α values defined, we can use it to obtain the estimated pixel \hat{f}_i by the equation

$$\hat{f}_i = \sum_{n=0}^{N-1} \alpha_n g[n], \quad (3)$$

where $g[0] \dots g[N-1]$ is a window of N pixels centered on the i -th pixel of observed image g in the lexicographic form. Using this approach, it is possible to make explicit the difference between Wiener Filter with Separable (SWF) and Isotropic MRF (IWF) in the autocorrelation matrix design. The idea is to define it based on an exponential decay model [13], [14].

In SWF, for each pixel (i, j) to be estimated, the autocorrelation matrix is defined as

$$R_{gg} = \begin{cases} \sigma_f^2(i, j) + \sigma_v^2(i, j), & \text{main diagonal} \\ \sigma_f^2(i, j)\rho_V^{|i'-i''|}\rho_H^{|j'-j''|}, & \text{remainder} \end{cases} \quad (4)$$

$$R_{ff} = (\sigma_f^2(i, j)\rho_V^{|i'-i|}\rho_H^{|j'-j|}) \quad (5)$$

where ρ_V and ρ_H are vertical and horizontal correlation coefficients that, for typical images, normally are chosen equal to 0.95 and (i', j') and (i'', j'') corresponds to pixel positions in a window.

In IWF, the autocorrelation matrix is defined as

$$R_{gg} = \begin{cases} \sigma_f^2(i, j) + \sigma_v^2(i, j), & \text{main diagonal} \\ \sigma_f^2(i, j)\rho^{\sqrt{(i'-i'')^2+(j'-j'')^2}}, & \text{remainder} \end{cases} \quad (6)$$

$$R_{ff} = (\sigma_f^2(i, j)\rho^{\sqrt{(i'-i)^2+(j'-j)^2}}) \quad (7)$$

where ρ is a correlation coefficient normally equal to 0.95. In this case, the influence of the central pixel circularly decays around it.

In both SWF and IWF, the statistics of the original image are computed as in the PWF.

IV. GENERALIZED WIENER FILTER

The Generalized Wiener Filter was designed in [15] based on Fisher Information minimization. The Fisher Information represents the amount of information that a given observed random variable conveys about an unknown parameter. An observed Information Fisher can be estimated on a Gaussian Markov Random Field (GMRF), with respect to a certain neighborhood system [15]. In this particular case, the parameter of interest is the spatial dependency that controls the structure of a GMRF. Essentially, the idea can be summarized as follows: in a GMRF, contextual patterns (patches) that are aligned to the global behavior have low value of observed Fisher information (because they exhibit high local likelihood). Therefore, modifying a given pixel in order to minimize the local observed Fisher information has the effect of smoothing image patches, since images typically show significant spatial correlation (which reflects in large values for the MRF spatial dependence parameter, guiding the global behavior).

Levada and Mascarenhas [15], through the Fisher Information on a GMRF, proposed a generalization of the Pointwise Wiener Filter, which is a particular case of proposed GWF method. Estimates of the noise-free pixels in this method are defined as [15], [16]

$$\begin{aligned} \hat{f}(i, j) = & \bar{f}(i, j) \\ & + \frac{\sigma_f^2(i, j)}{\sigma_f^2(i, j) + \sigma_v^2(i, j)} [\alpha(g(i, j) - \bar{g}(i, j))] \\ & + (1 - \alpha) \sum_{g(k, l) \in \eta(i, j)} (g(k, l) - \bar{g}_{\text{GMRF}}(i, j)), \end{aligned} \quad (8)$$

where $\alpha \in [0, 1]$ represents a balance between the pointwise filtering ($\alpha = 1$) and the contextual filtering ($\alpha = 0$), in other words, between local MSE minimization and local observed

Fisher Information minimization [15]. In addition, as in the Pointwise Wiener Filter we consider that under additive zero mean noise $\bar{g}(i, j) = \bar{f}(i, j)$ (this statistics is calculated using pre-smoothed version of the observed image or by a Non Local Means approach). On the other hand, \bar{g}_{GMRF} is a simple local average computed directly from the noisy observations. Recent results in audio denoising have shown that, in presence of AWGN, the use of GWF with $\alpha \neq 1$ overperforms the Pointwise Wiener Filter [16].

V. NON-LOCAL MEANS

The Non Local Means method was proposed by Buades et al [17] based mainly on the redundancy of patches in images. In this method, the noise-free estimated value of a pixel is basically defined as a weighted mean of pixels in a certain region. Regarding Additive White Gaussian Noise (AWGN), these weights are calculated using a Euclidean distance to measure the similarity between a central patch and neighboring patches in a search window, where the central pixel of both central patch and search window is the current pixel to be estimated. This method can be represented by the following equation [17]

$$\hat{f}_s = \frac{\sum_{t \in W} \omega(s, t) g_t}{\sum_{t \in W} \omega(s, t)}, \quad (9)$$

where \hat{f}_s is a current noise-free estimated pixel of the image, g_t is a noisy pixel belong to a search window W and $\omega(s, t)$ are the weight between the patches centralized in s and t and defined by [17]

$$\omega(s, t) = \exp\left(-\frac{1}{h} \sum_{k \in P} |g_{s,k} - g_{t,k}|^2\right), \quad (10)$$

where h controls the exponential decay, P are the patch indices and $g_{s,k}$ and $g_{t,k}$ are the k -th pixel in the patches s and t , respectively.

In this paper, we use a fast algorithm for Non Local Means Method proposed by Deledalle et al [18], with performance optimization based on convolution between a patch shape and similarity measures calculated by Fast Fourier Transform (FFT). Using patch shape beyond one classical square patch, it can reduce the rare patch effect, such as halo.

VI. THE PROPOSED METHODOLOGY

The Non Local Means method is a state-of-art method to denoise images corrupted by AWGN. However, despite the high capacity to reduce the noise, this method does not improve the contrast. In turn, the Wiener filter approaches change the contrast level, but the noise reduction is usually worse than in the NL Means.

Based on that, we investigate a way to join these methods in order to obtain a best trade-off between noise reduction and contrast improvement.

Thus, we propose to estimate the statistics as pre-estimated mean and variance for Wiener approaches on an estimate of the noise-free image given by the Non Local Means Method.

In order to evaluate the proposal, we use these contextual methods based on Wiener Filter and Markov Random Field to denoise CT images as described and discussed in next Section.

VII. EXPERIMENTS AND RESULTS

In this section, some experiments allowed us to compare the different approaches of the Wiener Filter described in this paper applied on CT images reconstructed by POCS (Projection onto Convex Sets) [6], [7], [8] or FBP (Filtered Backprojection) [2]. To measure quantitatively the performance of the methods, we calculated the Peak Signal-to-Noise Ratio (PSNR), a MSE based metric, and the Structural Similarity Index (SSIM) [19], which presents more fidelity with the human vision. Besides the denoising performance, the processing time was also shown in the results.

In addition, several parameters values are used. To obtain an estimate of the noise-free image by the mean filter, we use kernel sizes (K) 3×3 or 5×5 , whereas to obtain a Non Local Means pre-smoothing window search size (S) 10×10 and patch size (P) 3×3 were used. The window sizes (W) to estimate local variance and mean were 3×3 , 5×5 and 7×7 . Finally, for GWF values of alpha parameter between 0 (only context) and 0.9 with step size equal 0.1 and first ($V = 1$) and second ($V = 2$) order Markovian neighborhoods (define the patch) are tested.

Two phantoms are considered in these experiments. For each phantom, CT images were acquired with two different exposure times, 20 and 3 seconds, the first being considered the original image and the second the noisy image (lower dose), respectively.

The first phantom corresponds to the classical Shepp-Logan phantom to simulate the acquisition of head image [20]. This phantom is composed of homogeneous areas of different tonalities, sizes and shapes. The image reconstructed dimensions for this phantom were 128×128 pixels and the noise variance estimated in a homogeneous area was 0.0052 and 0.0094 for reconstructed image by POCS and FBP, respectively. The best results in terms of SSIM and PSNR for each method regarding this phantom are shown in Tables I and II, as well its denoised images in Figs. 1 and 2.

For this phantom reconstructed by POCS (Table I and Fig. 1), the best result in terms of both SSIM and PSNR is obtained by Non Local Means Method. Visually, there was a higher noise reduction by Non Local Means, but the best result obtained by GWF presents a suitable contrast.

For this phantom reconstructed by FBP (Table II and Fig. 2), the best result in terms of PSNR is obtained by GWF with first order neighborhood (4 nearest neighbors), a high level of contextual information ($\alpha = 0.1$), $W = 3 \times 3$ and statistics obtained from Non Local Means approach. This result is about 8.7 dB higher than the result obtained by Non Local Means method. In turn, the best result in terms of SSIM is obtained by SWF with $W = 5 \times 5$ and statistics also obtained from Non Local Means approach. Visually, we can note that a better trade-off between noise reduction and contrast was obtained

TABLE I

RESULTS FOR SHEPP-LOGAN PHANTOM RECONSTRUCTED BY POCS. THE SYMBOL * INDICATES THAT THE PRE-ESTIMATED STATISTICS ARE OBTAINED FROM THE NL MEANS RESULT (THE TIME FOR THESE RESULTS INCLUDE THE STATISTICS ESTIMATION TIME).

Methods	PSNR	SSIM	Time(s)
Noisy Image	22.44	0.53	-
NL Means ($S = 10 \times 10, P = 3 \times 3$)	24.30	0.75	0.79
PWF ($W = 7 \times 7, K = 3 \times 3$)	21.79	0.67	1.33
PWF ($W = 5 \times 5, K = 3 \times 3$)	21.74	0.67	1.32
PWF ($W = 5 \times 5$)*	21.90	0.71	1.92
PWF ($W = 3 \times 3$)*	21.53	0.72	1.91
IWF ($W = 7 \times 7, K = 3 \times 3$)	20.60	0.68	32.06
IWF ($W = 7 \times 7$)*	20.47	0.70	34.41
SWF ($W = 7 \times 7, K = 3 \times 3$)	20.94	0.52	42.10
SWF ($W = 5 \times 5, K = 3 \times 3$)	19.81	0.66	13.68
SWF ($W = 7 \times 7$)*	19.85	0.47	47.33
SWF ($W = 3 \times 3$)*	19.57	0.69	6.08
GWF ($\alpha = 0.7, V = 1, W = 5 \times 5, K = 3 \times 3$)	22.32	0.63	1.69
GWF ($\alpha = 0.9, V = 2, W = 5 \times 5, K = 3 \times 3$)	22.08	0.68	1.67
GWF ($\alpha = 0.8, V = 1, W = 5 \times 5$)*	22.93	0.72	2.27

TABLE II

RESULTS FOR SHEPP-LOGAN PHANTOM RECONSTRUCTED BY FBP. THE SYMBOL * INDICATES THAT THE PRE-ESTIMATED STATISTICS ARE OBTAINED FROM THE NL MEANS RESULT (THE TIME FOR THESE RESULTS INCLUDE THE STATISTICS ESTIMATION TIME).

Methods	PSNR	SSIM	Time(s)
Noisy Image	12.18	0.13	-
NL Means ($S = 10 \times 10, P = 3 \times 3$)	12.67	0.35	1.01
PWF ($W = 5 \times 5, K = 5 \times 5$)	17.23	0.52	1.88
PWF ($W = 3 \times 3$)*	20.47	0.62	2.60
IWF ($W = 7 \times 7, K = 3 \times 3$)	17.94	0.58	51.42
IWF ($W = 7 \times 7, K = 5 \times 5$)	17.13	0.59	51.35
IWF ($W = 3 \times 3$)*	19.74	0.65	6.86
IWF ($W = 5 \times 5$)*	18.58	0.69	17.77
SWF ($W = 5 \times 5, K = 3 \times 3$)	17.16	0.47	18.07
SWF ($W = 7 \times 7, K = 5 \times 5$)	16.77	0.55	56.60
SWF ($W = 3 \times 3$)*	19.86	0.66	6.67
SWF ($W = 5 \times 5$)*	19.36	0.71	17.87
GWF ($\alpha = 0.3, V = 1, W = 3 \times 3, K = 3 \times 3$)	17.72	0.38	2.28
GWF ($\alpha = 0.9, V = 2, W = 5 \times 5, K = 5 \times 5$)	17.06	0.51	2.32
GWF ($\alpha = 0.1, V = 1, W = 3 \times 3$)*	21.41	0.66	3.05
GWF ($\alpha = 0.7, V = 2, W = 3 \times 3$)*	20.59	0.66	3.05

by the contextual approaches with statistics obtained from Non Local Means approach.

The other phantom is composed of cylindrical structure of plexiglass with ten air filled holes of different diameters, arranged asymmetrically. Here, this phantom is called Asymmetric. The major motivation to use this phantom is to evaluate the capacity of the methods to preserve the resolution. The image reconstructed dimensions for this phantom were 100×100 pixels and the noise variance estimated in a homogeneous area was 0.0037 and 0.0126 for reconstructed image by POCS and FBP, respectively. The best results in terms of SSIM and PSNR for each method regarding this phantom are displayed in Tables III and IV, as well its denoised images in Figs. 3 and 4.

For this phantom reconstructed by POCS (Table III and Fig. 3), the best result in terms of both PSNR and SSIM was obtained by GWF with second order neighborhood (8 nearest neighbors), a low level of contextual information ($\alpha = 0.8$), $W = 3 \times 3$ and statistics obtained from Non Local Means approach. This result is about 3.7 dB higher than the result obtained by Non Locals Means method. Visually, we can note that a good noise reduction and a better contrast was obtained

by the best results. Besides, the results obtained by other contextual approaches (IWF and SWF) can be considered very good too.

For this phantom reconstructed by FBP (Table IV and Fig. 4), the best result in terms of PSNR is obtained by GWF with first order neighborhood (4 nearest neighbors), a low level of contextual information ($\alpha = 0.7$), $W = 5 \times 5$, $K = 3 \times 3$ and statistics obtained from pre-smoothed version of the observed image. This result is about 3.1 dB higher than the result obtained by Non Local Means method. In turn, the best result in terms of SSIM is obtained by IWF with $W = 3 \times 3$, SWF with $W = 3 \times 3$ and GWF with second order neighborhood (8 nearest neighbors), a low level of contextual information ($\alpha = 0.7$), all of them with statistics obtained from Non Local Means approach. Visually, we can note that a better trade-off between noise reduction and contrast was also obtained by the contextual approaches with statistics obtained from Non Local Means approach.

Regarding the processing time, all methods are mainly dependent of the window size (W), being the IWF and SWF more affected by this parameter. However, all methods are easily parallelizable. In general, the GWF method was faster

TABLE III

RESULTS FOR ASYMMETRIC PHANTOM RECONSTRUCTED BY POCS. THE SYMBOL * INDICATES THAT THE PRE-ESTIMATED STATISTICS ARE OBTAINED FROM THE NL MEANS RESULT (THE TIME FOR THESE RESULTS INCLUDE THE STATISTICS ESTIMATION TIME).

Methods	PSNR	SSIM	Time(s)
Noisy Image	22.17	0.64	-
NL Means ($S = 10 \times 10, P = 3 \times 3$)	23.90	0.81	0.67
PWF ($W = 3 \times 3, K = 5 \times 5$)	25.63	0.79	0.81
PWF ($W = 3 \times 3$)*	24.14	0.81	1.36
IWF ($W = 3 \times 3, K = 3 \times 3$)	24.23	0.77	2.27
IWF ($W = 5 \times 5, K = 3 \times 3$)	22.87	0.77	6.01
IWF ($W = 3 \times 3$)*	23.71	0.80	3.01
SWF ($W = 3 \times 3, K = 3 \times 3$)	24.34	0.77	3.08
SWF ($W = 5 \times 5, K = 3 \times 3$)	24.12	0.77	8.50
SWF ($W = 3 \times 3$)*	23.80	0.80	3.96
GWF ($\alpha = 0.9, V = 2, W = 3 \times 3, K = 5 \times 5$)	26.83	0.79	1.00
GWF ($\alpha = 0.8, V = 2, W = 3 \times 3$)*	27.58	0.81	1.55

TABLE IV

RESULTS FOR ASYMMETRIC PHANTOM RECONSTRUCTED BY FBP. THE SYMBOL * INDICATES THAT THE PRE-ESTIMATED STATISTICS ARE OBTAINED FROM THE NL MEANS RESULT (THE TIME FOR THESE RESULTS INCLUDE THE STATISTICS ESTIMATION TIME).

Methods	PSNR	SSIM	Time(s)
Noisy Image	16.32	0.28	-
NL Means ($S = 10 \times 10, P = 3 \times 3$)	17.86	0.38	1.31
PWF ($W = 3 \times 3, K = 3 \times 3$)	20.31	0.44	1.20
PWF ($W = 3 \times 3, K = 5 \times 5$)	16.85	0.45	0.81
PWF ($W = 3 \times 3$)*	18.11	0.46	1.99
IWF ($W = 3 \times 3, K = 3 \times 3$)	18.12	0.44	2.69
IWF ($W = 7 \times 7, K = 3 \times 3$)	16.84	0.45	22.63
IWF ($W = 7 \times 7$)*	16.66	0.45	23.91
IWF ($W = 3 \times 3$)*	16.21	0.47	3.86
SWF ($W = 3 \times 3, K = 3 \times 3$)	18.13	0.44	2.64
SWF ($W = 7 \times 7, K = 3 \times 3$)	17.90	0.45	34.61
SWF ($W = 7 \times 7$)*	17.59	0.45	27.69
SWF ($W = 3 \times 3$)*	16.21	0.47	3.91
GWF ($\alpha = 0.7, V = 1, W = 5 \times 5, K = 3 \times 3$)	20.96	0.44	1.43
GWF ($\alpha = 0.9, V = 1, W = 3 \times 3, K = 5 \times 5$)	16.84	0.45	1.39
GWF ($\alpha = 0.5, V = 1, W = 5 \times 5$)*	20.49	0.45	2.57
GWF ($\alpha = 0.7, V = 2, W = 3 \times 3$)*	16.74	0.47	2.63

than the other contextual Wiener filters.

VIII. CONCLUSIONS

In this paper, we proposed contextual denoising of CT images reconstructed by POCS or FBP using Markovian Wiener Filters and its parameter estimation based on Non Local Means approach. Experiments were performed regarding two phantoms acquired with different exposure times, high and low dose. The results showed that combination of Non Local Means approach, Wiener Filter and contextual modeling by Markov Random Fields produce a good balance between noise reduction and contrast level. Therefore, this proposal is suitable to denoise CT images.

Besides, the Generalized Wiener Filter with Non Local Means has shown the best performance in terms both quantitative and qualitative, outperforming the state-of-art Non Local Means method in some cases.

Future works include a detailed analysis of the noise presented in the image domain to check conditions such as signal-dependent behavior of the noise, an adaptive windowing technique for controlling the windows size (W) and an adaptive definition for the parameter α in the GWF.

ACKNOWLEDGMENT

The authors would like to thank Paulo E. Cruvinel for providing the CT phantoms, Charles Deledalle for providing the basic source code of his Non Local Means algorithm, FAPESP (São Paulo Research Foundation) for the financial support to Denis H. P. Salvadeo (grant number 2010/09248-7) and CNPq for the financial support to Alexandre L. M. Levada through the research grant number 475054/2011-3.

REFERENCES

- [1] N. Savage, "Medical imagers lower the dose," *IEEE Spectr.*, vol. 47, no. 3, pp. 14–15, 2010.
- [2] A. C. Kak and M. Slaney, *Principles of Computerized Tomographic Imaging*. IEEE Press, 1988.
- [3] C. L. Epstein, *Introduction to the mathematics of medical imaging*, 2nd ed. SIAM, 2008.
- [4] J. Giraldo, Z. Kelm, L. Guimaraes, L. Yu, J. Fletcher, B. Erickson, and C. McCollough, "Comparative study of two image space noise reduction methods for computed tomography: Bilateral filter and nonlocal means," in *31st Annual International Conference of the IEEE Engineering in Medicine and Biology Society 2009 (EMBC'2009)*, 2009, pp. 3529–3532.
- [5] R. Geraldo and N. Mascarenhas, "Noise reduction filters based on pointwise MAP for CT images," in *IEEE International Symposium on Circuits and Systems (ISCAS'2011)*, Rio de Janeiro, 2011, pp. 89–92.

- [6] F. V. Salina, “Métodos híbridos para reconstrução tomográfica de imagens usando POCS e teoria da estimação,” PhD Thesis, Instituto de Física de São Carlos, Universidade de São Paulo, São Carlos, 2007, (in portuguese).
- [7] F. V. Salina, N. D. A. Mascarenhas, and P. E. Cruvinel, “A comparison of POCS algorithms for tomographic reconstruction under noise and limited view,” in *Proceedings of the 15th Brazilian Symposium on Computer Graphics and Image Processing (SIBGRAPI'02)*, 2002, pp. 342–346.
- [8] F. V. Salina and N. D. A. Mascarenhas, “A hybrid estimation theoretic-POCS method for tomographic image reconstruction,” in *Proceedings of the XVIII Brazilian Symposium on Computer Graphics and Image Processing (SIBGRAPI'05)*, 2005, pp. 220–224.
- [9] C. S. Won and R. M. Gray, *Stochastic Image Processing*. Kluwer Academic/Plenum Publishers, 2004.
- [10] S. Z. Li, *Markov Random Field Modeling in Image Analysis*, 3rd ed. Springer, 2009.
- [11] D. T. Kuan, A. A. Sawchuk, T. C. Strand, and P. Chavel, “Adaptive noise smoothing filter for images with signal-dependent noise,” *IEEE Transactions on Pattern Analysis and Machine Intelligence*, vol. 7, no. 2, pp. 165–177, 1985.
- [12] S. M. Kay, *Fundamentals of statistical signal processing: estimation theory*. Prentice-Hall, 1993.
- [13] G. T. Zaniboni and N. Mascarenhas, “Fusão bayesiana de imagens utilizando coeficientes de correlação localmente adaptáveis,” in *IX Simpósio Brasileiro de Sensoriamento Remoto*. Santos: INPE, 1998, pp. 1003–1014, (in portuguese).
- [14] H. Zhang, A. Nosratinia, and J. Wells, R.O., “Modeling the autocorrelation of wavelet coefficients for image denoising,” in *2000 IEEE International Conference on Image Processing (ICIP'2000)*, 2000, pp. 304–307.
- [15] A. Levada and N. Mascarenhas, “Filtragem adaptativa de ruído gaussiano em imagens através da minimização da informação de Fisher observada,” in *VI Workshop de Visão Computacional (WVC'2010)*, Presidente Prudente, 2010, pp. 7–12, (in portuguese).
- [16] A. Levada and D. Correa, “An adaptive approach for contextual audio denoising using local Fisher information,” in *IEEE International Symposium on Circuits and Systems (ISCAS2011)*, 2011, pp. 125–128.
- [17] A. Buades, B. Coll, and J. M. Morel, “A review of image denoising algorithms, with a new one,” *SIAM Multiscale Modeling & Simulation*, vol. 4, no. 2, pp. 490–530, 2005.
- [18] C.-A. Deledalle, V. Duval, and J. Salmon, “Non-local methods with shape-adaptive patches (NLM-SAP),” *Journal of Mathematical Imaging and Vision*, pp. 1–18, 2011.
- [19] Z. Wang and A. Bovik, “Mean squared error: Love it or leave it? a new look at signal fidelity measures,” *IEEE Signal Processing Magazine*, vol. 26, no. 1, pp. 98–117, 2009.
- [20] L. Shepp and B. Logan, “The Fourier reconstruction of a head section,” *IEEE Transactions on Nuclear Science*, vol. 21, pp. 21–43, 1974.

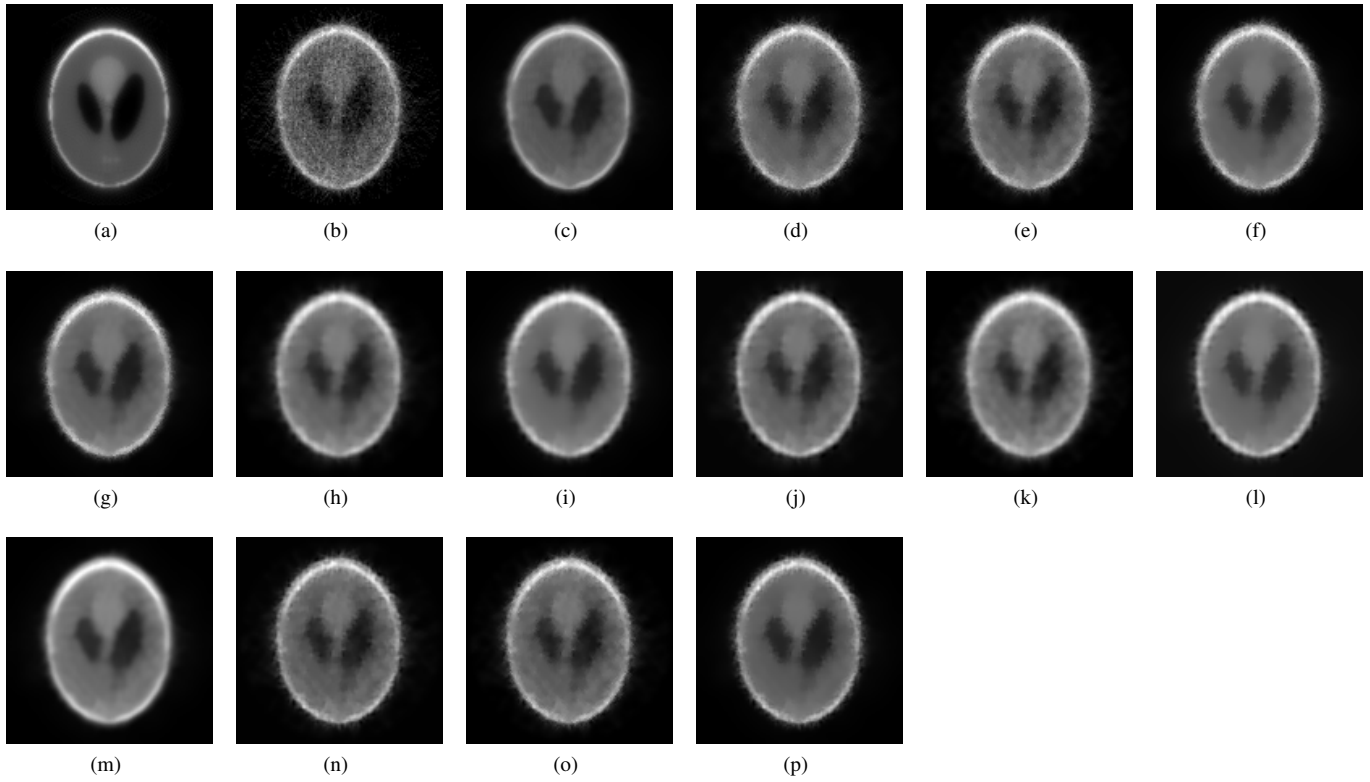


Fig. 1. Denoised images for Shepp-Logan phantom reconstructed by POCS: (a) original image, (b) noisy image, (c) NL Means result, (d)-(g) PWF results, (h)-(i) IWF results, (j)-(m) SWF results and (n)-(p) GWF results in the same order of Table I.

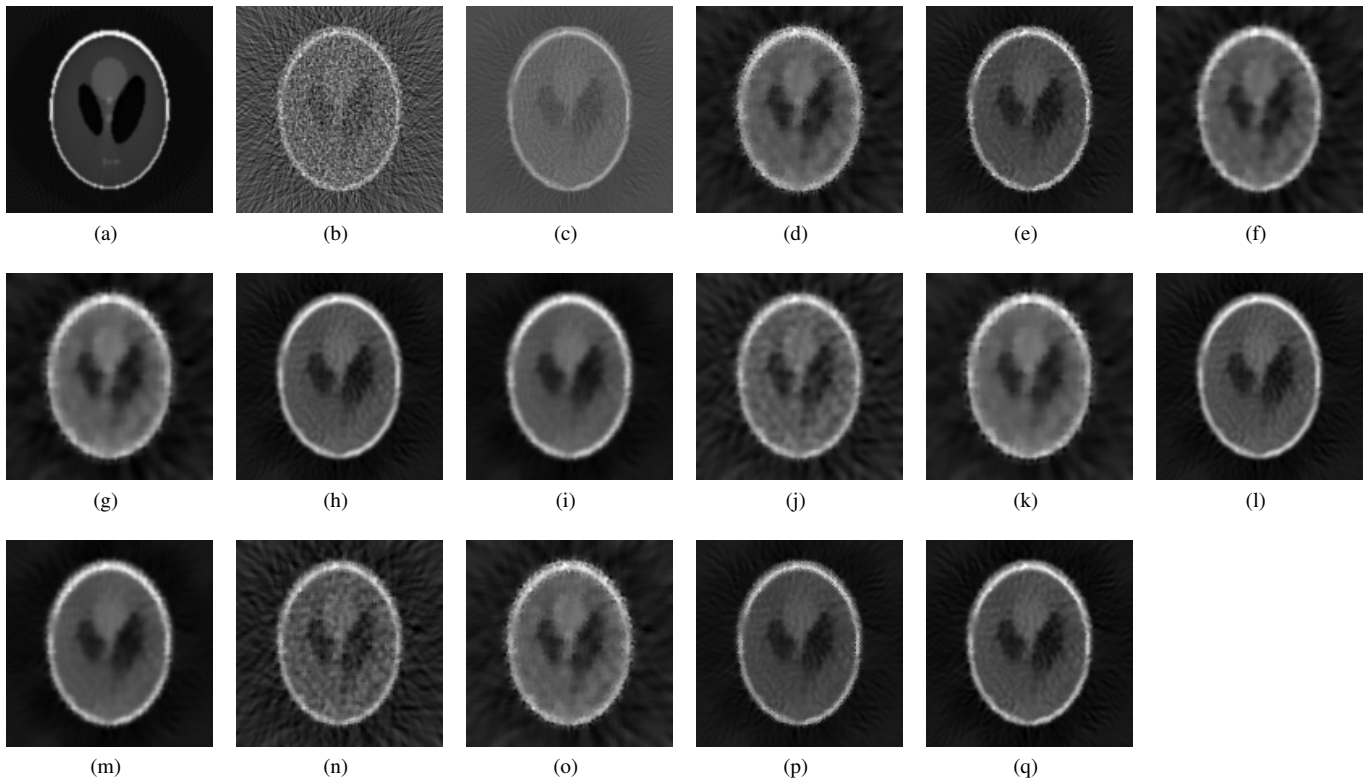


Fig. 2. Denoised images for Shepp-Logan phantom reconstructed by FBP: (a) original image, (b) noisy image, (c) NL Means result, (d)-(e) PWF results, (f)-(i) IWF results, (j)-(m) SWF results and (n)-(q) GWF results in the same order of Table II.

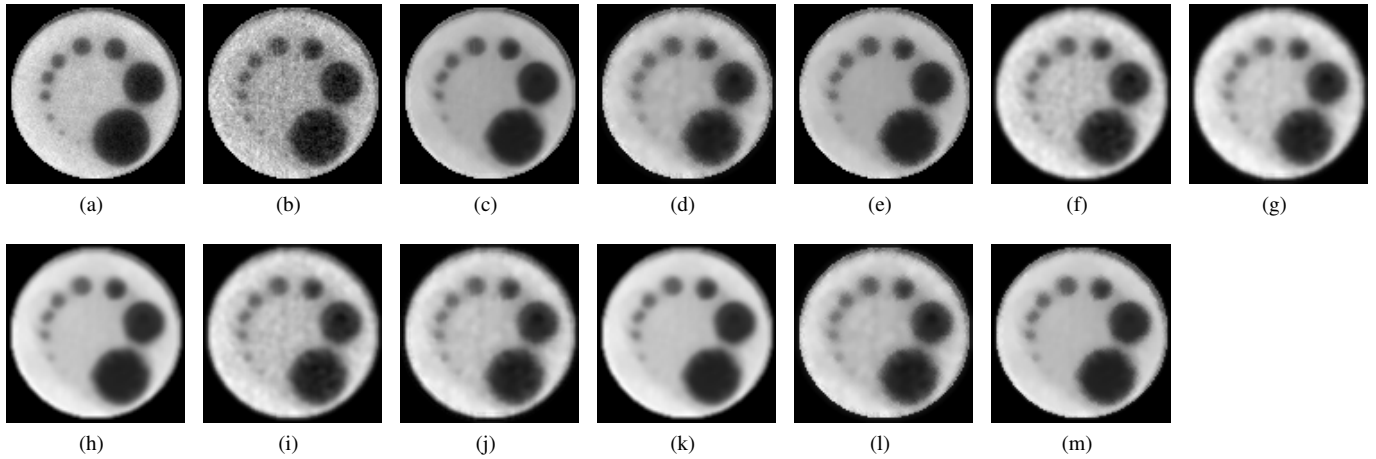


Fig. 3. Denoised images for Asymmetric phantom reconstructed by POCS: (a) original image, (b) noisy image, (c) NL Means result, (d)-(e) PWF results, (f)-(h) IWF results, (i)-(k) SWF results and (l)-(m) GWF results in the same order of Table III.

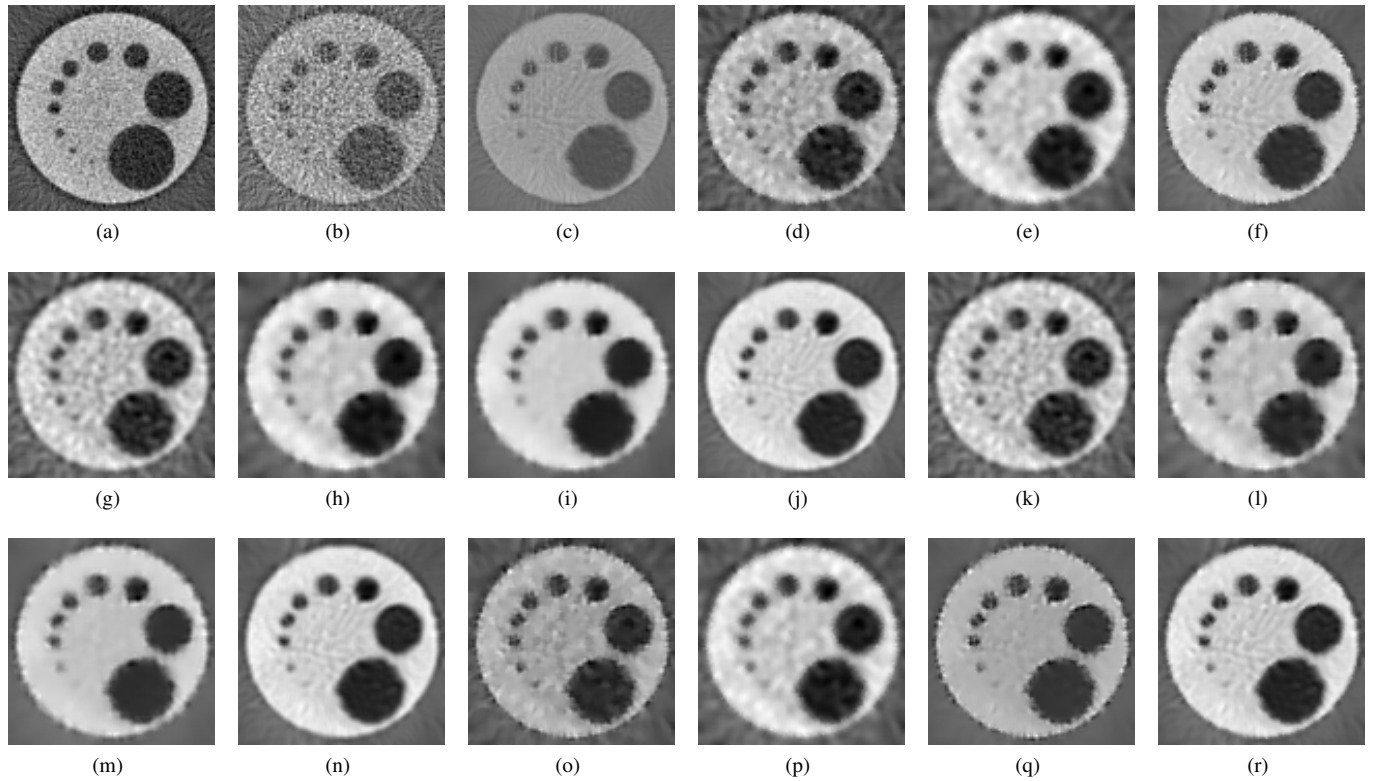


Fig. 4. Denoised images for Asymmetric phantom reconstructed by FBP: (a) original image, (b) noisy image, (c) NL Means result, (d)-(f) PWF results, (g)-(j) IWF results, (k)-(n) SWF results and (o)-(r) GWF results in the same order of Table IV.